A&A 424, 325–330 (2004)
DOI: 10.1051/0004-6361:20035893

Astronomy & Astrophysics

Sublimating components in the coma of comet C/2000 WM_1 (LINEAR)⋆

G. P. Tozzi[1], L. M. Lara[2], L. Kolokolova[3], H. Boehnhardt[4], J. Licandro[5], and R. Schulz[6]

[1] INAF – Osservatorio Astrofisico di Arcetri, Largo E. Fermi 5, 50125 Firenze, Italy
e-mail: tozzi@arcetri.astro.it
[2] Instituto de Astrofísica de Andalucía, CSIC, PO Box 3004, 18080 Granada, Spain
e-mail: lara@iaa.es
[3] University of Florida, Gainesville, FL 32611, Florida, USA
e-mail: ludmilla@astro.ufl.edu
[4] Max-Planck-Institut für Astronomie, Königstuhl 17, 69117 Heidelberg, Germany
e-mail: hboehnha@mpia-hd.mpg.de
[5] Isaac Newton Group of Telescopes & Instituto de Astrofísica de Canarias, 38700 Santa Cruz de la Palma, Tenerife, Spain
e-mail: licandro@ing.iac.es
[6] Research and Scientific Support Department of ESA, ESTEC, Keplerlaan 2, 2200AG Noordwijk, The Netherlands
e-mail: Rita.Schulz@esa.int

Received 17 December 2003 / Accepted 4 May 2004

Abstract. Comet C/2000 WM_1 (LINEAR) was observed at ESO at the time of its closest approach to the Earth at the beginning of December 2001 (geocentric distance: 0.32 AU). The aim of the observations was characterization of the solid component of the coma. Observations have been acquired over a wide spectral range, from the visible to the thermal infrared using three telescopes simultaneously. In this paper we discuss the possible discovery of two sublimating components in the coma, one of them with scattering properties very different from those of the "common" cometary dust. We provide evidence that these two components possibly originate from different kinds of organic material.

Key words. comets individual: C/2000 WM_1 (LINEAR)

1. Introduction

Comet C/2000 WM_1 (LINEAR) (hereafter C/WM_1) was discovered on Dec. 16, 2000 with the Lincoln Near Earth Asteroid Research (LINEAR) program of MIT (IAUC # 7546, 2000).

According to early predictions, the comet was going to become a bright object ($V \approx 5$) at the time of its closest approach to the Earth (geocentric distance, $\Delta = 0.32$ AU), at the beginning of December 2001. Hence, it was possible to observe the comet with high spatial resolution and high S/N.

We planned to perform simultaneous observations with three telescopes for three successive nights at that time at La Silla (ESO). The planned observations were the following: in the visible with the 1.5 m Danish telescope, in the near-IR with the New Technology Telescope (NTT) and in the thermal IR with the 3.6 m. Unfortunately, bad weather and technical problems prevented us from taking data during the second night and for most of the last one. Table 1 gives the geometry of the comet during the observations.

⋆ Based on observations collected at the European Southern Observatory, Chile. Program 68.C-0506.

Table 1. Observing geometry for C/2000 WM_1 (LINEAR).

Date	r_h (AU)	Δ (AU)	ϕ (deg)	PA (deg)
Dec. 2, 2001	1.21	0.32	38.4	62.2
Dec. 4, 2001	1.18	0.32	45.7	60.8

Abbreviations: r_h = heliocentric distance (AU); Δ = geocentric distance (AU); ϕ = comet phase angle, PA = the position angles of the extended Sun→target radius vector.

The main aim of the observations was the study of the solid component in the inner coma at high spatial resolution and within a wide spectral range (0.4–20 μm). Since different properties of dust grains are responsible for the scattered solar light and for the emission of radiation over different spectral ranges, simultaneous observations with the three telescopes would allow us to obtain maximum information on the properties of the dust. In particular, we planned to map dust properties, such as albedo, and correlate them with morphological properties, such as jets, fans, etc.

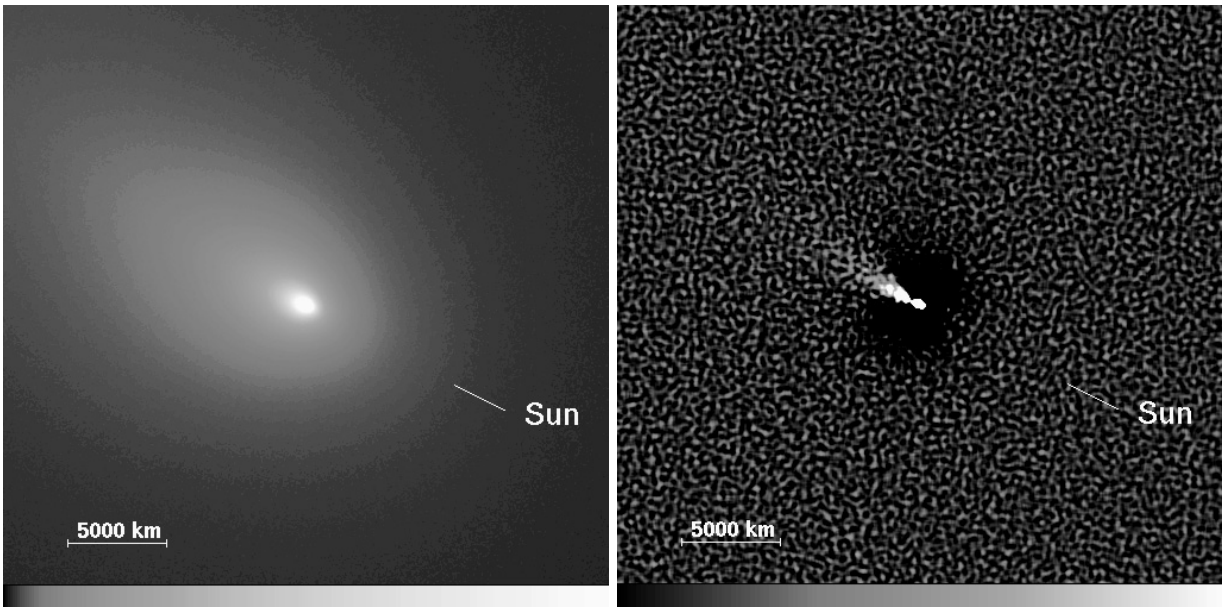

Fig. 1. The Coma of Comet C/2000 WM$_1$ (LINEAR): original image (*left*) in J band of Dec. 2, calibrated in Af (scale $-0.1-10\times10^{-6}$) in logarithmic scale, and (*right*) the same image adaptive Laplace filtered, in linear scale. North is up, East to the left; field of view is $\sim$30 000 $\times$ 30 000 km^2; the photometric nucleus is at the center of the field of view; the scale size and Sun direction are also shown. Apart from a tail structure which is visible in the anti-Sun direction of the filtered image, no other details were detectable.

Preliminary results and observations in the visible have been presented already (Tozzi et al. 2002; Lara et al. 2002, 2004). In this paper we deal with the possible discovery of two short-lifetime solid components.

2. Observations and data reduction

As mentioned earlier, bad weather conditions prevented us from making observations during the 2nd night and most of the 3rd one. Due to the high proper motion of the comet ($\approx$620″/h), there were also tracking problems with the 1.5D and 3.6 m telescopes. In the visible, only some images and one spectrum turned out to be of good quality. Moreover, because of a technical problem, no spectroscopic measurements were acquired in the thermal-IR. Complete analysis of the optical data can be found in Lara et al. (2004).

In this paper we will discuss the results obtained from the broad-band images in the scattering regime, i.e. in the R, I, J, H and K bands. The other images have not been used for this analysis due to the lower S/N of the narrow band images, and to the different mechanism of emission of the thermal-IR images.

After correcting for bias and flat field by the usual way, all the images were sky subtracted. The sky background was obtained at the edges of the frames acquired in the optical range, and in regions about 8′ away from the comet in the images taken in the near-IR. After re-centering all the frames on the photometric nucleus, a second order sky subtraction was performed by using the plot of ΣAf (proportional to the area covered by grains multiplied by the average albedo A, see below) as a function of ρ, that is very sensitive to sky residual at large nucleocentric distances (ρ). Finally the images acquired with the same filter and on the same night were median averaged, to increase the S/N in the region far from the nucleus, and calibrated in Af.

To find possible structures in the coma, we analyzed the images by using the Laplace filter technique (see for example Boehnhardt & Birkle 1994). As indicated in Fig. 1, apart from a small tail structure in the anti-Sun direction, the comet appears featureless in all images.

The $Af\rho$ parameter was introduced by A'Hearn et al. (1984) in order to give an observational quantity related to the solid component production that was, at first order, independent of the aperture used. The ΣAf that is proportional to the column density of the solid component at a nucleocentric distance ρ has been recently introduced (Tozzi & Licandro 2002). It is the azimuthal averaged $Af(\rho)$ multiplied by the area covered by an annulus of radius ρ and depth equal to 1 cm. Practically, it is obtained from observations by calibrating the images (with "intensity" in Af and axis in projected distance) and by integrating the Af in the annulus of variable radius. ΣAf and $Af\rho$ are, at first order, constant with ρ for a "normal" cometary coma described by a simple outflow law (i.e. a coma with a $1/\rho$ radial profile). Jets and fans do not change the trend of the functions, as long as the solid components produced by them expand as the square of the nucleocentric distance and the production is constant with time, with a timescale of the order of the transit time of the dust in the FOV of the images.

The solar radiation pressure may have some effects on the ΣAf function since it changes the outflow velocity of the particles with an acceleration depending on their size. However, we evaluated that the effect is negligible for nucleocentric distances smaller than approximately 10^4 km, where the effect of radiation pressure on the velocity of particles of different size is small in respect to their original terminal velocities;

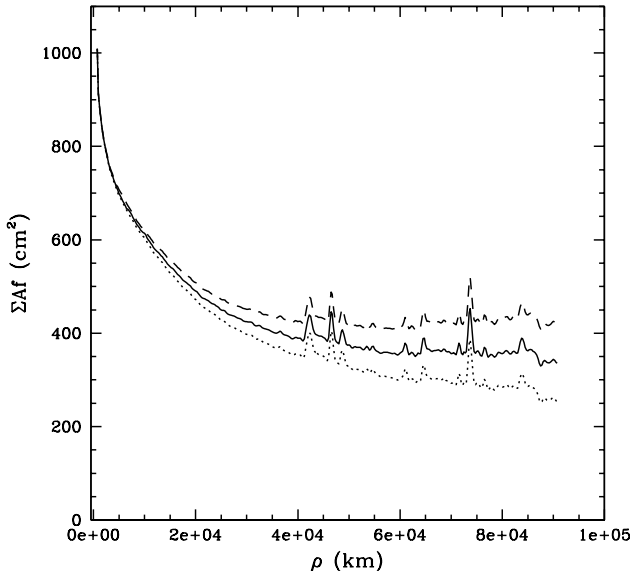

Fig. 2. Example of ΣAf profiles. Solid line represents the function with the "good" sky background subtracted. Dotted and dashed lines have been obtained after subtracting background varied by ±2% of the "good" one. The spikes in the functions are due to stars in the field.

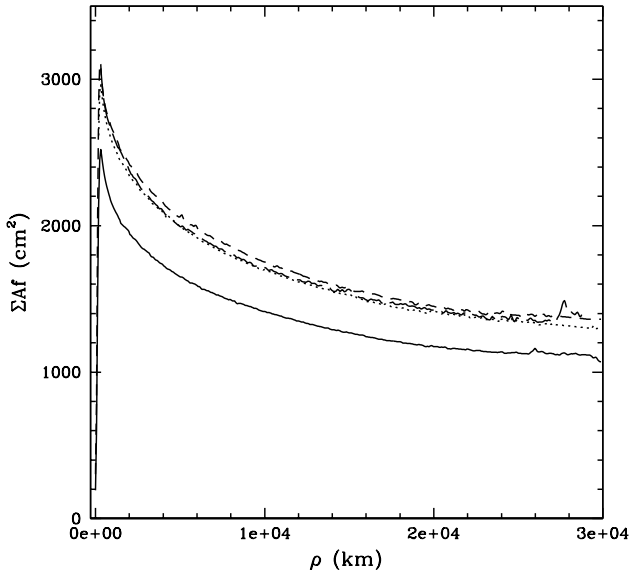

Fig. 3. Example of ΣAf profiles for J (full line), H (dotted line) and K (dashed line) for observation of Dec. 2. The profile for H for Dec. 4 is also plotted (long dashed). The latter is practically coincident with the equivalent profile of Dec. 2.

the azimuthal averaging further reduces the radiation pressure effect on the spatial distribution.

ΣAf, contrary to $Af\rho$, is very sensitive to intensity variations, such as residual sky background, that can be described as a function linearly dependent on ρ; sudden changes in activity like outbursts, that would produce a double exponential profile that moves away from the nucleus with time; sublimating components or dust fragmentation that would lead to a decrease or an increase of the function with ρ. Examples of ΣAfs for a comet with a "normal" coma and for a comet with strong outbursts can be found in Lara et al. (2003) and Tozzi & Licandro (2002), respectively.

Figure 2 shows the sensitivity of ΣAf to small variations of the sky level: the solid line indicates the function after the subtraction of what we consider as the best value of the sky; dotted and dashed lines are the same functions with the sky value increased and decreased by 2% of its actual value, respectively. These 2% variations correspond to 1.67×10^{-4} times the value of the maximum intensity of the comet. As it can be seen in the figure, these small variations of the background produce strong effects in the profiles, but affect mainly the outer part, i.e. the component independent of ρ (ΣAf_0, see below). Of course, column density of the solid component that changes linearly with ρ would be wrongly interpreted as sky background. However, no physical phenomenon that we can think of can change the column density linearly with ρ. Even in the case of ice grains studied long ago by Delsemme & Miller (1971), the grain sizes were predicted to decrease linearly with time. This means that, at first order, the filling factor f of a single grain would decrease with the square of time, and, assuming some mean outflow velocity, with the square of ρ, until its complete sublimation. For that reason we believe that the linear dependence of ΣAf on ρ is only due to sky residual and that this method allows us to precisely evaluate the sky background, even when the coma fills almost all the image.

Because the profiles of sporadic phenomena (change of activity...) and steady ones (sublimation...) may be similar, the only way to distinguish between them is by observing the comet on different nights. In our case the resulting ΣAf profiles versus ρ are very steep in the inner coma as can be seen in Fig. 3. The fact that the images obtained during the third night have the same profiles excludes sporadic phenomena as a possible cause. If this was the case, a larger $Af\rho$ or a peak moving outward should be seen. The most obvious explanation is that the filling factor f was decreasing due to some sublimating components, such as ices, organic solids, and dust covered by ice or organic material. Other causes, for example, an acceleration of the dust in the inner part, are less probable, but cannot be excluded a priori.

All the measured ΣAf profiles can be well fitted by the following function

$$\Sigma Af = \Sigma Af_0 + \Sigma Af_1 e^{-\rho/L_1} + \Sigma Af_2 e^{-\rho/L_2} \quad (1)$$

i.e. by a constant term ΣAf_0, representing the normal long-lived cometary coma (simple outflow model), plus two exponential functions of ρ, with intensities equal to ΣAf_1 and ΣAf_2 and scalelength L_1 and L_2, respectively. This relationship reproduces observed values very well and all the values of ΣAfs and L_s for the different nights are very similar. To increase the S/N in the outer part of the coma, to reduce the contribution of the background stars and to have the maximum extension of the coma, all the images in the same band, recorded during all the nights, were median averaged. The ΣAfs were then measured and fitted for these five (R, I, J, H and K) resulting images.

Figure 4 gives an example of the measured and fitted functions (upper panel) and the relative error (bottom panel).

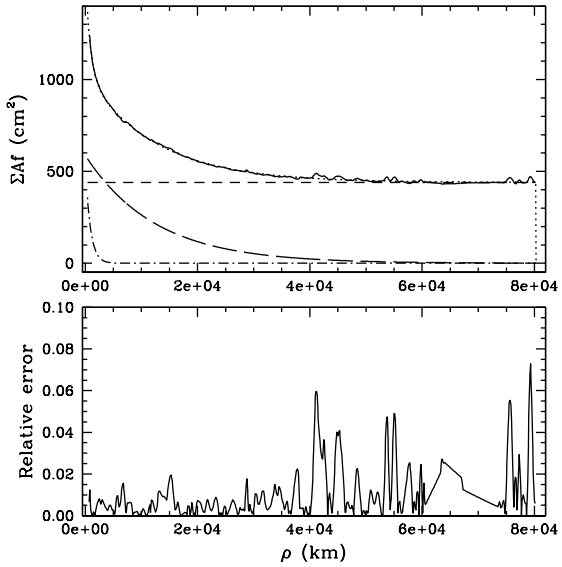

Fig. 4. *Upper panel*: example of fitting of the ΣAf function (I band). The full line represents the measured function and, almost coincident, the one computed by the fitting procedure (dotted line). Dashed, dotted-dashed and long-dashed lines are the refractory, the long and short scalelengths component, respectively. Lower panel gives the relative error. Usually it is less than 1−2%. Higher values are due to field stars.

The fitting is very good and the measured and fitted functions are indistinguishable. The relative error is always less than 2%, apart from the region where the measured function increases because of the residual field stars.

Assuming that the albedo A does not change with ρ, the ΣAf is proportional to the column density of the components, and assuming the same three components (one constant and two exponential) in the spatial density (number of dust grains per cm^{-3}), by numerically integrating along the line of sight it is possible to establish that both the spatial density and the column density have the same exponential profile, but the scalelengths are ≈25% longer than those for the column density, i.e. in the ΣAf.

The resulting scalelengths (L_1 and L_2) and ΣAfs at $\rho = 0$ for all the components and bands are given in Table 2. We point out that the scalelength of the longer sublimating component (L_1) may have a large systematic error in the R band, because of gas contamination present here (see Lara et al. 2004). Since the lifetimes of the contaminating gases (mainly C_2 and NH_2) are of the order of 10^4 s and their velocities are of the order of 1 km s^{-1}, the effect is more important for the profile of the component with longer scalelength, but it is negligible for the short scalelength and for the non-sublimating ones. The errors given in the table are from the fitting procedure. The errors due to the flux calibration, that affect only the ΣAfs but not the scalelengths, are estimated to be ≈5%. The average scalelengths, excluding that measured in the R band, are $L_1 = 9800 \pm 1300$ km and $L_2 = 750 \pm 120$ km. Taking into account the 25% difference mentioned above, the scalelengths for the densities are equal to $12\,250 \pm 1625$ km and 940 ± 150 km, for the long and short scalelengths components, respectively.

Table 2. Values of ΣAfs and scalelengths (L_s) obtained from the fitting of the ΣAf vs. ρ functions.

	ΣAf_0 cm^2	ΣAf_l cm^2	L_l km	ΣAf_s cm^2	L_s km
R	367 ± 1	474 ± 4	17582 ± 243	533 ± 59	759 ± 68
I	379 ± 1	466 ± 5	11979 ± 160	483 ± 31	939 ± 63
J	1071 ± 1	1066 ± 2	9118 ± 44	599 ± 8	693 ± 13
H	1235 ± 2	1266 ± 3	9721 ± 58	607 ± 9	790 ± 19
K	1355 ± 2	1342 ± 4	8399 ± 55	666 ± 20	569 ± 22

The absence of expanding structures in the comet images hampers our effort to measure the outflow velocity of these solid components. It is well known that the outflow velocity of the cometary solid component depends on the drag force of the gas which, in turn, depends on the gas production rate and on the size of the grains. For example, Combi et al. (1997) have shown that in comet Hale-Bopp small grains (0.1 μm) can reach terminal outflow velocities similar to that of the gas (≈0.8 km s^{-1}). In our case the gas production rate was much lower, of the order of 3×10^{28} s^{-1} (Schleicher et al. 2002), than in the case of Hale-Bopp and the grains cannot be much smaller than 1 μm to efficiently scatter the solar radiation in the near-IR. In presence of a given size distribution, the smaller grains would have a terminal velocity higher than the bigger ones, but in the case of a non-variable solid component production this would not result in any size differentiation with ρ. In the case of sublimating grains the smaller ones will have also a shorter lifetime because the sublimation rate depends on the exposed area (i.e. $\propto r^2$, with "r" the size of the grain) and the amount of material depends on volume (i.e. $\propto r^3$). So the two processes compete and, if the higher speed for small grains tends to increase the scalelength, the shorter lifetime tends to decrease it. A better solution of these problems would require the use of a coma model, but this is beyond the purpose of the present paper. Then, in order to derive an order of magnitude of the lifetimes involved, we assumed a mean terminal velocity of the grains of ≈0.2 km s^{-1} (see, for example, Combi & Fink 1997). The resulting lifetimes of the two sublimating components are about 61 000 s (17 h) and 4700 s (1.3 h), respectively. We point out that this result is based also on the assumption of a symmetric outflow in space. In the case that the sublimating components are confined in jets and/or fans directed close to the line of sight, these values would lower the limits, since the real scalelength could be longer than the projected one. However, since the images taken on Dec. 2 and 4 do not show any difference, this would be valid only in the exceptional cases of a nucleus rotational period commensurable with 48 h or with a polar jet/fan and rotational axis directed along the line of sight.

Figure 5, left panel, gives the colors of the three solid components, where the ΣAfs of Table 2, i.e. the ΣAfs at $\rho = 0$, are plotted as a function of the central wavelength of the filters used. The non-sublimating and long lifetime components have similar scattering properties: both colors are very red, showing a strong increase with wavelength, i.e. the behavior

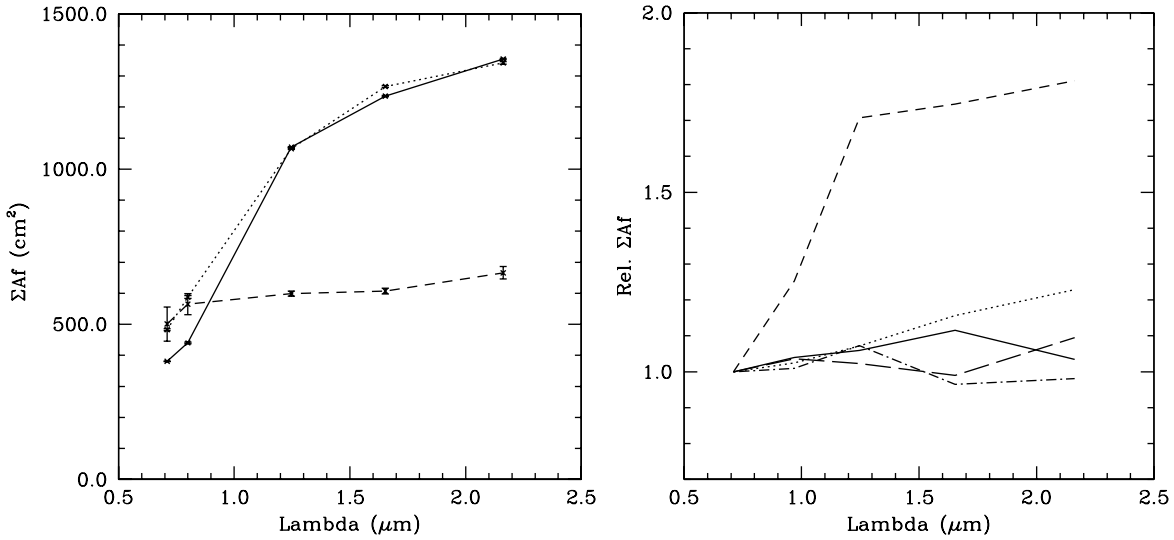

Fig. 5. *Left*: measured ΣAf for the three solid states in R, V, J, H, K. Solid line is for the non-sublimating component, dotted and dashed lines are respectively for the long and short lifetime sublimating components. *Right*: spectral trend of various organic materials: full, dotted, dashed, long dashed, dot-dashed lines are for water ice, laboratory organics, EURECA organics, tholin and kerogen, respectively (see text).

typical of the "normal" cometary dust (Jewitt & Meech 1986). On the other hand, the short lifetime component has very different scattering properties with the albedo almost independent of wavelength.

3. Discussion

Even though other possible mechanisms cannot be excluded, our interpretation is that we have detected two solid sublimating components with different lifetimes. The first obvious explanation may be that these solid sublimating components are icy grains released by the nucleus. The existence of a water ice halo has been postulated long ago (Huebner 1966; Delsemme 1969) to explain the large water production rates measured in some comets with nuclei too small for such production. A recent example is Comet C/1996 B2 (Hyakutake) with a $Q(H_2O)$ of $\approx 3 \times 10^{29}$ mol/s (Schleicher & Osip 2002) and a nucleus diameter of 3 km (Harmon et al. 1997). Hanner et al. (1981) showed that dirty ice grains would have very short lifetimes at 1 AU from the Sun, of the order of a few hundreds of seconds, depending on their size. Pure ice grains, with a very low absorption coefficient, may have very long lifetimes, varying from $\approx 5 \times 10^3$ s for grains with radius equal to 1 μm to several billions of seconds for grains of radius of 50 μm. It is also possible that the ice is embedded in fluffy silicate grains, as suggested by Gunnarsson (2003). In such a way, the grains will release the icy material without changing their dimension. However, in this case the lifetime of the ice would be very short, as pointed out also by Lien (1990) and Gustafson (1994), and the water would be released in bursts, since the silicate grains with embedded ice are heated very efficiently. We conclude then that, unless we have pure water grains, the sublimating material cannot be identified as water ice.

It is more likely that these components are organic volatiles. The presence of two solid components with different lifetimes, i.e. with different sublimation rates, implies the presence of two types of organic volatiles. It can be seen from Fig. 5, left panel, that these two components differ not only in their lifetime but also in the spectral trend of the scattered light. This can indicate different spectral dependencies of their optical constants and, thus, can be used to figure out their nature. We calculated spectral trends in the intensity of the scattered light modeling the dust as an ensemble of spherical particles with a power-law size distribution of the form $n(r) \propto r^{-a}$ where n is the number of particles of a given radius r; the calculations were made for $a = 3.0$ and $a = 2.75$ according to the results of Kolokolova et al. (2001). We considered several sublimating materials: ice and a variety of organic materials, namely, tholin (Khare et al. 1984), kerogen (Khare et al. 1990), laboratory organics (Jenniskens 1993), and EURECA organics (Li & Greenberg 1997). The best fit to the observed trend was obtained at $a = 2.75$ for the short-lifetime component using the laboratory organics and for the long-lifetime component using the EURECA organics (Fig. 5, right panel). The difference between these two organic materials is that the laboratory organics by Jenniskens (1993), so-called "first generation" organics, are produced by irradiation of a mixture of gases (H_2O, CO, CH_4, NH_3) in the laboratory, whereas the EURECA organics, the "second generation" ones, result from exposing the laboratory-created residues to the solar ultraviolet irradiation on the EURECA satellite for 6 months (Li & Greenberg 1997). Thus, the EURECA organics represents more processed organics, already having experienced the solar irradiation that could make it less volatile. This may explain why the observed dust component that has a spectral trend similar to the EURECA organics has a longer lifetime in comparison to the organics that have a spectral trend more typical of less processed, laboratory organics. It is also possible, as suggested by Combi & Fink (1997) to explain the parent of C_2, that the grains had a core-mantle structure with the materials indicated before covering

a refractory core. Recently Cottin et al. (2004) have proposed that the parent of the extended source of formaldehyde may be a refractory organic, the polyoxymethylene. We cannot prove that, but we can point out that the scalelengths that they compute for pure organic grains and for an heterogeneous mixture of organic and silicate components are in the order of magnitude of the scalelength that we measure for our short lifetime components.

This comet did not show any other abnormal characteristics: it was not at its first passage in the inner solar system; no dust jets and/or fans are present; the relative abundance of the minor species is "typical" (Schleicher et al. 2002); the comet can be classified in the high polarization class (Joshi et al. 2003). Also the very long scalelength of the parent of C_2 necessary to fit its profile with ρ and the production rate of C_2 (Lara et al. 2004), that is supposed to have some organic solid state as parent, (Combi & Fink 1997) seems not very unusual.

4. Conclusions

From observations of comet C/2000 WM_1 it has been shown that the ΣAf profiles in the inner part of the coma are very steep, much steeper than that of a coma described by a simple outflow model. This has been interpreted as indicating the presence of two sublimating solid components of scalelengths equal to 12 250 and 940 km. Assuming a velocity of the solid components of the order of 0.2 km s^{-1}, the lifetime of these two components would be 61 000 s and 4700 s, respectively. Water ice grains can be excluded since their lifetime would be much shorter than these values. It is more reasonable to assume organic material, that may have lifetimes comparable with the measured ones and that have the spectral trend in agreement with the measured one.

Even if we cannot give an indisputable answer on the nature of these two sublimating components, this is the first time that these components have been detected so clearly. Further observations of this kind are necessary for other bright comets that will pass close to the Earth, to check whether C/WM_1 is peculiar or if similar components exist in other long period or new comets.

References

A'Hearn, M. F., Schleicher, D. G., Millis, R. L., Feldman, P. D., & Thompson, D. T. 1984, AJ, 89, 579
Boehnhardt, H., & Birkle, K. 1994, A&A, 107, 101
Combi, M. R., Kabin, K., DeZeeuw, D. L., Gombosi, T. I., & Powell, K. G. 1997, EM&P, 79, 275
Combi, M. R., & Fink, U. 1997, ApJ, 484, 879
Cottin, H., Bénilan, Y., Gazeau, M.-C., & Raulin, F. 2004, Icarus, 167, 397
Delsemme, A. H. 1969, in Extraterrestrial Matter, ed. C. A. Randall, 304
Delsemme, A. H., & Miller, D. C. 1971, Panet. Space Sci., 19, 1259
Gunnarsson, M. 2003, A&A, 398, 353
Gustafson, B. A. S. 1994, AREPS, 22, 553
Hanner, M. S. 1981, Icarus, 47, 342
Harmon, J. K., Ostro, S. J., Benner, L. A. M., et al. 1997, Science, 278, 1921
Huebner, W. F., & Weigert, A. 1966, Z. Astrophys., 64, 185
Jenniskens, P. 1993, A&A, 274, 653
Jewitt, D., & Meech, K. J. 1986, ApJ, 310, 937
Joshi, U. C., Baliyan, K. S., & Ganesh, S. 2003, A&A, 405, 1129
Khare, B. N., Sagan, C., Arakawa, E. T., et al. 1984, Icarus, 60, 127
Khare, B. N., Sagan, C., Arakawa, E. T., et al. 1990, Lunar and Planetary Science Conf., 21, 627
Kolokolova, L., Lara, L.-M., Schulz, R., Stüwe, J., & Tozzi, G. P. 2001, Icarus, 153, 197
Lara, L.-M., Licandro, J., di Martino, M., & Tozzi, G. P. 2002, ESA SP-500, 709
Lara, L.-M., Licandro, J., & Tozzi, G. P. 2003, A&A, 404, 373L
Lara, L.-M., Tozzi, G. P., Boehnhardt, H., di Martino, M., & Schulz, R. 2004, A&A, submitted
Li, A., & Greenberg, J. M. 1997, A&A, 323, 566L
Lien, D. 1990, ApJ, 355, 680
Meier, R., Eberhardt, P., Krankowsky, D., & Hodges, R. R. 1993, A&A, 277, 677
Schleicher, D. G., & Osip, D. J. 2002, Icarus, 159, 210
Schleicher, D. G., Woodney, L., & Birch, P. V. 2002, EM&P, 90, 401
Tozzi, G. P., Boehnhardt, H., Campins, H., et al. 2002, ESA SP-500, 593
Tozzi, G. P., & Licandro, J. 2002, Icarus, 157, 187